Available online at www.sciencedirect.com
SciVerse ScienceDirect
Acta Materialia 61 (2013) 4542–4558
Acta MATERIALIA
www.elsevier.com/locate/actamat

A micromechanical analysis of the coupled thermomechanical superelastic response of textured and untextured polycrystalline NiTi shape memory alloys

Reza Mirzaeifar [a], Reginald DesRoches [b], Arash Yavari [a,b,*], Ken Gall [a,c]

[a] George W. Woodruff School of Mechanical Engineering, Georgia Institute of Technology, Atlanta, GA 30332, USA
[b] School of Civil and Environmental Engineering, Georgia Institute of Technology, Atlanta, GA 30332, USA
[c] School of Materials Science and Engineering, Georgia Institute of Technology, Atlanta, GA 30332, USA

Received 18 February 2013; received in revised form 5 April 2013; accepted 9 April 2013
Available online 15 May 2013

Abstract

In this paper a micromechanical model that incorporates single crystal constitutive relationships is used for studying the pseudoelastic response of polycrystalline shape memory alloys (SMAs). In the micromechanical framework, the stress-free transformation strains of the possible martensite twinned structures, correspondence variant pairs (CVPs), obtained from the crystallographic data of NiTi are used, and the overall transformation strain is obtained by defining a set of martensitic volume fractions corresponding to active CVPs during phase transformation. The local form of the first law of thermodynamics is used and the energy balance relation for the polycrystalline SMAs is obtained. Generalized coupled thermomechanical governing equations considering the phase transformation latent heat are derived for polycrystalline SMAs. A three-dimensional finite element framework is used and different polycrystalline samples are modeled based on Voronoi tessellations. By considering appropriate distributions of crystallographic orientations in the grains obtained from experimental texture measurements of NiTi samples, the effects of texture and the tension–compression asymmetry in polycrystalline SMAs are studied. The interaction between the stress state (tensile or compressive), the number of grains and the texture on the mechanical response of polycrystalline SMAs is studied. It is found that the number of grains (or size) affects both the stress–strain response and the phase transformation propagation in the material. In addition to tensile and compressive loadings, textured and untextured NiTi micropillars with different sizes are also studied in bending. The coupled thermomechanical framework is used for analyzing the effect of loading rate and the phase transformation latent heat on the response of both textured and untextured samples. It is shown that the temperature changes due to the heat generation during phase transformation can affect the propagation of martensite in samples subjected to high strain rates.

Keywords: Polycrystalline; Shape memory alloy; Phase transformation; Texture; Thermomechanical coupling

1. Introduction

Shape memory alloys (SMAs), particularly the near-equiatomic TiNi alloys, are currently used in applications in a wide variety of devices. SMA materials used in most applications are polycrystalline in nature. The cast SMA materials contain a random distribution of crystal orientations in the grains. However, in most applications, SMAs are processed by casting, followed by hot-working (i.e. drawing or rolling) and suitable heat treatments [44]. It is known that the deformation processing has a significant effect on the response of polycrystalline SMAs. For example, while the material response for a cast NiTi sample is almost symmetric in tension and compression, a cast, hot rolled, then cold drawn material exhibits a very large asymmetry in tension–compression response [8]. In some special

* Corresponding author at: School of Civil and Environmental Engineering, Georgia Institute of Technology, Atlanta, GA 30332, USA.
E-mail address: arash.yavari@ce.gatech.edu (A. Yavari).

1359-6454/$36.00 © 2013 Acta Materialia Inc. Published by Elsevier Ltd. All rights reserved.
http://dx.doi.org/10.1016/j.actamat.2013.04.023

samples, the maximum transformation strain in tension is reported to be more than two times the maximum transformation strain in compression for the hot rolled, then cold drawn material, with a significant difference between the stress levels in the stress–strain plateau [8]. This significant tension–compression stress–strain asymmetry in processed SMAs is due to the strong crystallographic texture. Gall and Sehitoglu [11] studied the role of texture on tension–compression asymmetry in polycrystalline NiTi. The crystallographic texture of some NiTi samples was determined by X-ray diffraction. The samples they studied were cold drawn, annealed, straightened, centerless ground, aged for 0.25 h at 550 °C and machined into dog-bone-shaped specimens with the loading axis parallel to the drawing direction. It was shown that for these samples the majority of the grains are oriented along the [1 1 1] crystallographic direction, which is soft under tensile loading and hard under compression. As a result of this textured orientation, a significant tension–compression asymmetry is observed in the stress–strain response of NiTi samples.

Macroscopic phenomenological constitutive frameworks are efficient tools for modeling the mechanical or thermomechanical response of polycrystalline SMAs in engineering applications [43,18,38,34,29]. However, these models are not appropriate for modeling the response of SMAs at the microscale, and consequently are not able to model some important aspects of the response of SMAs, such as the phase transformation initiation and propagation among the grains. As already mentioned, the crystallographic texture is a key property in studying polycrystalline SMAs. A simplified method for studying the role of texture on the mechanical response of polycrystalline SMAs is to use phenomenological constitutive equations and selecting appropriate transformation functions for modeling the asymmetry in SMAs [4,38]. However, a more precise analysis of the crystallographic texture and its effects on the thermomechanical response can only be achieved by using constitutive models based on the micromechanics of single crystals for studying polycrystal structures [10,45]. In these models, a polycrystalline material can be modeled by assigning a separate crystal orientation to each grain. Using this method, a preferred orientation of the crystallographic texture can be modeled, which leads to the actual thermomechanical response of polycrystalline SMAs without using an approximate phenomenological framework.

In the micromechanical models, the overall transformation strain is related to the stress-free transformation strains of all the correspondence martensite variant pairs (CVPs) obtained from the crystallographic data by using a volume fraction coefficient for each variant. Some studies based on these micromechanical models ignore the microstructure of grains and the intergranular interactions by using different averaging schemes [42,35,24,11,7]. Although these models are appropriate for studying the global response of the material, and are capable of analyzing important properties such as the role of texture on the tension–compression asymmetry [11], the grain boundary interactions and the intergranular effects are not considered in these models. To further understand the behavior of polycrystalline SMAs, it is necessary to use the micromechanical constitutive frameworks in conjunction with an accurate model of microstructure by simulating the polycrystal as a cluster of grains. The finite element method is an efficient tool for studying polycrystalline SMAs using the micromechanical framework. Gall et al. [10] and Lim and McDowell [22] employed three-dimensional finite element modeling to examine the thermomechanical behavior of a polycrystalline NiTi SMA in the pseudoelastic regime. In these works, a simplified geometric model was used in which all the grains are assumed as identical hexagonal prisms. Thamburaja and Anand [44] used a crystal-mechanics-based constitutive framework and the finite element modeling for studying the effect of crystallographic texture on the response of polycrystalline SMAs. They modeled the microstructure in the polycrystal by treating all the grains as cubes stacked adjacent to each other, forming a larger cube representing the polycrystal structure. A similar microstructure was used for studying the superelastic behavior of textured NiTi polycrystalline materials in tension–torsion [45] and the thermal effects in the superelasticity of crystalline SMAs [1]. To further understand the intergranular interactions in polycrystalline SMAs, we use a more realistic polycrystal structure by implementing Voronoi tessellations to generate the polycrystalline grain structure of microscaled NiTi SMAs.

Another significant contribution of the present work is in presenting an accurate thermomechanical framework for studying the effect of phase transformation latent heat in polycrystalline SMAs. There are several attempts in the literature for coupling the latent heat effect to the mechanical response of polycrystalline SMAs. A group of these works use the averaging schemes in studying the polycrystal and, because the physical shape of grains is not modeled, the temperature should also be studied as an averaged parameter in the whole material [7]. In another attempt to better understand the thermomechanical response of polycrystalline SMAs, Anand and Gurtin [1] coupled the energy balance equation with the mechanical constitutive relations for the simplified microstructure model with cubic grains and studied the strain rate effect on the response of NiTi SMAs. Lim and McDowell [22] introduced a simplified expression for the volumetric heat generation due to phase transformation and studied the coupled thermomechanical response of textured polycrystal samples in which the microstructure was constructed by identical grains as hexagonal prisms. It was assumed that the volumetric heat generation is proportional to the rate of change of overall martensitic volume fraction by using a constant relating the heat generation to the sum of the rate of martensitic volume fraction changes in all the active variants. In this paper, we use a comprehensive description of the energy balance equation in SMAs for calculating the latent heat during phase transformation. It will be shown that the volumetric heat generation/absorption is related to the rate of change of martensitic volume fractions

and stress. Derivatives of the latent heat with respect to temperature and strain are also calculated for implementation in an incremental finite element framework.

Several case studies are considered in this paper to help further understand some of the important phenomena in the thermomechanical response of polycrystalline SMAs. The role of texture on tension–compression asymmetry is studied and it is shown that adding more grains with a favorable crystal orientation changes the semi-symmetric response of an untextured sample toward an asymmetric response observed in single crystals. The effect of crystallographic texture on the phase transformation initiation and propagation is studied and it is shown that, while the phase transformation propagates almost equally in tension and compression for an untextured material, the spatial distribution of the martensite phase is remarkably more rapid in compression when the grains have a favorable [1 1 1] crystallographic orientation.[1] The effects of size and the number of grains on the mechanical response of polycrystalline SMAs subjected to both tensile and compressive loads are studied and it is shown that the number of grains has a strong effect on the initiation of phase transformation at the grain boundaries and the propagation of martensite region inside the polycrystal. Some case studies are presented for microscaled polycrystalline beams subjected to bending and it is shown how the stress and martensitic volume fraction distributions are affected by the texture in the beam. The load–deflection responses of textured and untextured beams in bending are also compared. The thermomechanical response of polycrystalline SMAs is studied by implementing the coupled energy balance and constitutive equations. It is shown that the latent heat is the cause of rate dependency in the response of SMAs at the microscale. It is also shown that the effect of loading rate on changing the slope of stress–strain plateau and changing the hysteresis area is consistent with the results previously observed at the macroscale. The effect of latent heat on the propagation of phase transformation between the grains is also studied, and it is shown that the phase transformation is slightly suppressed in fast loadings due to the temperature changes. The temperature changes at the microscale are compared with those obtained previously at the macroscale based on experimental observations and phenomenological modelings. It is shown that the temperature changes at different scales have similarities.

This paper is organized as follows. In Section 2 a micromechanical-based constitutive model for polycrystalline SMAs is presented. The thermomechanical coupling is discussed in Section 3. Details of the finite element framework, modeling grains based on Voronoi tessellations and the method of assigning appropriate crystallographic orientations in the textured and untextured materials are given in Section 4. The numerical results are presented in Section 5. Conclusions are given in Section 6.

[1] It is worth noting that the spatial spread of phase transformation initiation is more rapid in tension, as reported by Gall et al. [10]. However, we study the propagation of martensitic volume fraction as a function of average strain, as discussed in Section 5.2.

2. Constitutive modeling

In recent years, several different classes of constitutive models have been introduced for studying SMAs. Some of these models are developed for studying the macroscopic behavior of polycrystalline SMAs. Phenomenological macroscopic constitutive models are derived by using the Gibbs free energy as the thermodynamic potential and choosing an appropriate set of internal state variables to describe a measure of phase transformation. In these models evolution equations are postulated for the internal variables (i.e. the martensitic volume fraction and the transformation strain) and the second law of thermodynamics is used in order to find thermodynamic constraints on the material constitutive equations [20,43,38]. In this work, we consider a micromechanical model in which the transformation strain is related to the crystallographic data. Experimental and theoretical data are used to find the stress free transformation strain of martensite variants exactly [27,6]. The macroscopic transformation strain is considered as a sum of different active transforming martensite variants and the contribution of each variant is related to the total strain by the volume fraction of that specific variant [25,26,22,11]. The general micromechanical framework is briefly discussed next. It is worth noting that the austenite to martensite phase transformation in the constitutive framework of this paper is rate-independent in nature and possible effects of strain rate on the transformation are ignored. However, the thermomechanical coupling and the effect of phase transformation latent heat causes the material response to be rate dependent which is not directly caused by the rate dependency of the martensitic transformation.

2.1. The micromechanical framework

We use the micromechanical framework of Patoor et al. [36]. This model was used by Gall and Sehitoglu [11] to study the role of texture in tension–compression asymmetry in polycrystalline NiTi using an averaging scheme. It was also implemented in a three-dimensional finite element formulation for studying the cyclic thermomechanical behavior of polycrystalline pseudoelastic SMAs [22] based on a simplified model of the grains in the microstructure. The stress-free transformation strain corresponding to the nth martensite variant is given by

$$\hat{\epsilon}^n_{ij} = \frac{1}{2} g \left(l^n_i d^n_j + d^n_i l^n_j \right) \tag{1}$$

where d is the transformation direction, l is the habit plane normal and g is the transformation magnitude. We consider the $B2 \rightarrow B19'$ martensitic transformation for NiTi. Theoretically, there are 192 possible variants in NiTi by considering type I and type II twins [22], and this number is even larger when considering the compound twinning in NiTi [14,47]. However, it has been observed that type II-1

is by far the most prominent twinning mode in NiTi [32], and calculating the transformation strain by considering the active CVPs of this type results in a very good agreement between experimental observations and theoretical predictions [11,7,39,22]. In this case, the number of martensite variants for transformation is $1 \leqslant n \leqslant 24$ and the habit plane and transformation direction components are obtained from the crystallographic data (see Table 1 in [11]). The transformation magnitude for this case is $g = 0.1308$. The total transformation strain in a single grain is the sum of transformation strains from all martensite variants. By defining a martensitic volume fraction corresponding to each variant, the volume averaged transformation strain is given by[2]

$$\epsilon_{ij}^{t} = \sum_{n=1}^{24} \hat{\epsilon}_{ij}^{n} \xi^{n}, \tag{2}$$

where ξ^n is the volume fraction of the nth martensite variant. The total martensitic volume fraction is $\xi = \sum_{n=1}^{24} \xi^n$. The total volume fraction and the volume fraction of each variant are always between 0 and 1. For a single crystal, several free energy functions have been reported in the literature [35,11,7,1]. In this paper, we use the Gibbs free energy G for developing the coupled thermomechanical constitutive framework for studying polycrystalline SMAs. To obtain this function, we use the appropriate terms from the complementary free energy Ψ ($\Psi = -G$) introduced by Patoor et al. [35] and the appropriate terms for the thermal free energy given by Anand and Gurtin [1] in the Helmholtz free energy $\hat{\psi}$ for polycrystalline SMAs. The Gibbs free energy is given by:

$$\begin{aligned} G(\boldsymbol{\sigma}, T, \xi^n) = & -\frac{1}{2}\boldsymbol{\sigma} : \mathbb{S} : \boldsymbol{\sigma} \\ & - \boldsymbol{\sigma} : \sum_{n=1}^{24} \hat{\boldsymbol{\epsilon}}^{n} \xi^{n} + \beta(T - T_0) \sum_{n=1}^{24} \xi^{n} - \boldsymbol{\sigma} : \boldsymbol{\alpha}(T - T_0) \\ & + \rho c \left[(T - T_0) - T \ln\left(\frac{T}{T_0}\right) \right] + \sum_{m,n=1}^{24} H_{nm} \xi^{n} \xi^{m} \end{aligned} \tag{3}$$

where $\mathbb{S}$, $\boldsymbol{\sigma}$, T, T_0, $\hat{\boldsymbol{\epsilon}}^n$ and ξ^n are the compliance tensor, local stress tensor, temperature, reference temperature, transformation strain and martensitic volume fraction on the nth variant, respectively. The parameter β is a material constant, $\boldsymbol{\alpha}$ is the thermal expansion coefficient tensor and c is the specific heat.[3] The last term in Eq. (3) is an approximation that accounts for martensite variant interactions by introducing an interaction matrix H [36,35]. The terms in this matrix represent the interaction energy due to the formation of multiple interacting martensite CVPs. The incompatible CVPs are mutually transformed with a higher interaction energy compared to the compatible CVPs. Compatible CVPs have a smaller net intrinsic shear strain compared to incompatible CVPs, and the crystallographic data can be used for finding the compatible and incompatible pairs. However, we use a simplified method based on the strain compatibility equation, as expressed in detail by Gall and Sehitoglu [11]. Also, the interaction energies for the compatible and incompatible CVPs are assumed to be constant and temperature independent (Table 2 in [11]), which is shown to give accurate results compared to the experimental measurements [35,11,7,22]. The interface energies are ignored in this model. This is reasonable as the interface energies between the twin-related variants can be ignored because of the compatibility at the interface. The austenite (A)–martensite (M) interface energy is remarkably small compared to the other terms in the energy so it can be ignored [15,37,23]. However, it should be noted that, although these energies can be ignored at the microscale, they play an important role at the nanoscale [19,16].

By defining a deriving force f_n for each variant as

$$f_n = -\frac{\partial G}{\partial \xi_n} = \boldsymbol{\sigma} : \hat{\boldsymbol{\epsilon}}^{n} - \sum_{m=1}^{24} H_{nm} \xi^{m} - \beta(T - T_0) \tag{4}$$

the criteria for forward transformation of austenite to the nth martensite variant is given by $f_n = f^{am}$ and the condition for reverse transformation of the nth martensite variant to austenite is expressed as $f_n = f^{ma}$, where f^{am} and f^{ma} are critical energies for A to M and M to A transformations, respectively. During the forward and reverse phase transformations, the consistency condition $\dot{f}_n = 0$ is written as

$$\frac{\partial f_n}{\partial \boldsymbol{\sigma}} : \dot{\boldsymbol{\sigma}} + \frac{\partial f_n}{\partial T} : \dot{T} + \sum_{m=1}^{24} \frac{\partial f_n}{\partial \xi^{m}} \dot{\xi}^{m} = 0. \tag{5}$$

By substituting Eq. (4) into Eq. (5), the consistency condition can be rewritten as

$$\dot{\boldsymbol{\sigma}} : \hat{\boldsymbol{\epsilon}}^{n} - \sum_{m=1}^{24} H_{nm} \dot{\xi}^{m} - \beta \dot{T} = 0. \tag{6}$$

The condition (6) will be used in the next section for finding the incremental change of volume fraction of all the active variants during the phase transformation. It is worth noting that $\dot{\xi}$ is nonzero only for the active variants that satisfy the forward or reverse transformation conditions for the deriving force (4) and it is computationally more efficient to write the summations only on the active variants in developing the numerical algorithm.

2.2. The mechanical and thermal Jacobians

We use a finite element framework for modeling polycrystalline SMAs. For developing an incremental

[2] Although the phase transformation induced deformation is inhomogeneous at the microscale, it can be assumed that the deformation is averaged over a sufficiently large element that guaranties a smooth response during phase transformation [44].

[3] The parameters $\boldsymbol{\alpha}$ and c may be considered as functions of the martensitic volume fraction. However, for the SMAs used in practical applications these parameters are independent of the volume fraction and we have considered them constant throughout this paper, e.g. $\boldsymbol{\alpha} = \boldsymbol{\alpha}^A = \boldsymbol{\alpha}^M$ [38,28].

displacement based finite element, in addition to the constitutive relations given in the previous section, the tangent stiffness (mechanical Jacobian) and thermal moduli tensors are also needed. In order to obtain these tensors, the constitutive model of the SMA material should be linearized and represented as an incremental form. Deriving the mechanical Jacobian is given briefly in the following. More details of deriving the Jacobians are given by Lim and McDowell [22].

For an infinitesimal time increment, Δt, the time rate of each parameter $\mathscr{P}$ can be approximated by $\dot{\mathscr{P}} = \Delta\mathscr{P}/\Delta t$. Using this approximation, Eq. (6) can be written as a set of q simultaneous Eqs. ($1 \leqslant q \leqslant 24$ is the number of variants that satisfy the transformation conditions (4)):

$$\Delta\boldsymbol{\sigma} : \hat{\boldsymbol{\epsilon}}^n = \sum_{m=1}^{24} H_{nm}\Delta\xi^m + \beta\Delta T \tag{7}$$

Using this approximation, the stress increment is related linearly to the increment of temperature and the martensitic volume fraction of active variants. It can be shown that the martensitic volume fraction increment is also related to the strain increment linearly [22]. The stress increment can be approximated by

$$\Delta\boldsymbol{\sigma} = \frac{\partial\Delta\boldsymbol{\sigma}}{\partial\Delta\boldsymbol{\epsilon}} : \Delta\boldsymbol{\epsilon} + \frac{\partial\Delta\boldsymbol{\sigma}}{\partial\Delta T}\ \Delta T \tag{8}$$

where $\partial\Delta\boldsymbol{\sigma}/\partial\Delta\boldsymbol{\epsilon}$ is the mechanical Jacobian. The stress increment can be written as

$$\Delta\boldsymbol{\sigma} = \mathbb{S}^{-1} : \left(\Delta\boldsymbol{\epsilon} - \sum_{m=1}^{24}\Delta\boldsymbol{\epsilon}^m\right) \tag{9}$$

where $\boldsymbol{\epsilon}^i$ is the contribution of transformation strain from the ith martensite variant that is related to the stress-free transformation strain of the corresponding variant through the volume fraction as $\boldsymbol{\epsilon}^i = \hat{\boldsymbol{\epsilon}}^i\xi^i$. Substituting Eq. (9) into Eq. (7), one obtains

$$\mathbb{S}^{-1} : \left(\Delta\boldsymbol{\epsilon} - \sum_{m=1}^{24}\hat{\boldsymbol{\epsilon}}^m\Delta\xi^m\right) : \hat{\boldsymbol{\epsilon}}^n = \sum_{m=1}^{24} H_{nm}\Delta\xi^m + \beta\Delta T \tag{10}$$

By defining a transformation matrix Γ and a driving force vector F as

$$\Gamma_{mn} = \hat{\boldsymbol{\epsilon}}^m : \mathbb{S}^{-1} : \hat{\boldsymbol{\epsilon}}^n + H_{mn}, \quad F_m = \hat{\boldsymbol{\epsilon}}^m : \mathbb{S}^{-1} : \Delta\boldsymbol{\epsilon} - \beta\Delta T \tag{11}$$

the set of q simultaneous Eq. (10) can be rewritten in the matrix form as

$$[\Gamma]\{\Delta\xi\} = \{F\} \tag{12}$$

where the size of vectors and the transformation matrix depends on the number of active variants (q) and $\{\Delta\xi\}$ is a vector containing the incremental change of volume fraction of all the active variants. This set of equations will be used for calculating the incremental change of volume fractions.

For deriving the mechanical Jacobian, the incremental stress–strain relation (9) is differentiated with respect to the strain increment as

$$\frac{\partial\Delta\boldsymbol{\sigma}}{\partial\Delta\boldsymbol{\epsilon}} = \mathbb{S}^{-1} : \left(\mathbb{I} - \sum_{m=1}^{24}\frac{\partial\Delta\boldsymbol{\epsilon}^m}{\partial\Delta\boldsymbol{\epsilon}}\right) \tag{13}$$

where $\mathbb{I}$ is the identity tensor. The derivative of the transformation strain with respect to the total strain can be written as

$$\frac{\partial\Delta\boldsymbol{\epsilon}^m}{\partial\Delta\boldsymbol{\epsilon}} = \frac{\partial\Delta\boldsymbol{\epsilon}^m}{\partial\Delta\xi^m} \otimes \frac{\partial\Delta\xi^m}{\partial\Delta\boldsymbol{\epsilon}} = \boldsymbol{\epsilon}^m \otimes \Gamma^{-1}_{mn}\frac{\partial F^n}{\partial\Delta\boldsymbol{\epsilon}} \tag{14}$$

where $\otimes$ denotes the tensor product, and the last term is derived using the inverse of Eq. (12). Substituting Eq. (14) into Eq. (13) gives the mechanical Jacobian to be implemented in the finite element formulation. The thermal Jacobian is obtained by differentiating Eq. (9) with respect to the temperature increment as

$$\frac{\partial\Delta\boldsymbol{\sigma}}{\partial\Delta T} = \mathbb{S}^{-1} : \left(-\sum_{m=1}^{24}\frac{\partial\Delta\boldsymbol{\epsilon}^m}{\partial\Delta T}\right) \tag{15}$$

where the derivative of the transformation strain with respect to temperature is calculated using the chain rule as

$$\frac{\partial\Delta\boldsymbol{\epsilon}^m}{\partial\Delta T} = \frac{\partial\Delta\boldsymbol{\epsilon}^m}{\partial\Delta\xi^m}\frac{\partial\Delta\xi^m}{\partial\Delta T} = \hat{\boldsymbol{\epsilon}}^m\Gamma^{-1}_{mn}\frac{\partial F^n}{\partial\Delta T} \tag{16}$$

Substituting Eq. (16) into Eq. (15) gives the thermal Jacobian. Details of implementing the calculated Jacobians and the constitutive equations into the user subroutine (UMAT) in the finite element program is given by Lim and McDowell [22] as a computational step-by-step algorithm. For algorithmic details of the time integration procedure for a rate-independent single-crystal constitutive model for SMAs, readers are referred to [44]; their model is based on the algorithm developed by Anand and Kothari [2] for rate-independent crystal plasticity.

3. Thermomechanical coupling

We generalize the thermomechanical framework presented by Lim and McDowell [22] in this section by considering a comprehensive description of the energy balance equation for obtaining the thermal coupled equations. It will be shown that the method of relating the latent heat linearly to the rate of change of martensitic volume fraction is a simplification of this general model by ignoring some terms in the energy balance equation. We use a similar method as used previously by the authors for obtaining the governing thermomechanical equations based on phenomenological constitutive models for SMAs [28,30].

The coupled thermomechanical governing equations for SMAs are derived by considering the first law of thermodynamics in local form as

$$\rho\dot{u} = \boldsymbol{\sigma} : \dot{\boldsymbol{\epsilon}} - \operatorname{div}\boldsymbol{q} + \rho\hat{g} \tag{17}$$

where ρ is the mass density and u is the internal energy per unit mass. The parameters $\boldsymbol{q}$ and $\hat{g}$ are the heat flux and internal heat generation. The dissipation inequality reads

$$\rho\dot{s} + \frac{1}{T}\ \mathrm{div}\ \boldsymbol{q} - \frac{\rho\hat{g}}{T} \geqslant 0 \tag{18}$$

where s is the entropy per unit mass. Substituting the following definition of Gibbs free energy

$$G = \rho u - \boldsymbol{\sigma} : \boldsymbol{\epsilon} - \rho s T \tag{19}$$

into the dissipation inequality, the second law of thermodynamics reads

$$-\dot{G} - \dot{\boldsymbol{\sigma}} : \boldsymbol{\epsilon} - \rho s \dot{T} \geqslant 0 \tag{20}$$

Using the definition of the Gibbs free energy (3), the time derivative of G is given by

$$\dot{G} = \frac{\partial G}{\partial \boldsymbol{\sigma}} : \dot{\boldsymbol{\sigma}} + \frac{\partial G}{\partial T}\dot{T} + \sum_{n=1}^{24} \frac{\partial G}{\partial \xi^n} : \dot{\xi}^n \tag{21}$$

Substituting Eq. (21) into Eq. (20) gives

$$-\left(\frac{\partial G}{\partial \boldsymbol{\sigma}} + \boldsymbol{\epsilon}\right) : \dot{\boldsymbol{\sigma}} - \left(\frac{\partial G}{\partial T} + \rho s\right)\dot{T} - \sum_{n=1}^{24} \frac{\partial G}{\partial \xi^n} : \dot{\xi}^n \geqslant 0 \tag{22}$$

The validity of Eq. (22) for all $\dot{\boldsymbol{\sigma}}$ and $\dot{T}$ implies the following constitutive equations:

$$-\frac{\partial G}{\partial \boldsymbol{\sigma}} = \boldsymbol{\epsilon}, \quad -\frac{\partial G}{\partial T} = \rho s \tag{23}$$

The energy balance equation is obtained by substituting Eqs. (23) and (21) into Eq. (17) as

$$\rho T\dot{s} = -\sum_{n=1}^{24} \frac{\partial G}{\partial \xi^n}\dot{\xi}^n - \mathrm{div}\boldsymbol{q} + \rho\hat{g} \tag{24}$$

The constitutive relation $(23)_2$ is used for calculating the time derivative of the specific entropy as

$$\rho\dot{s} = -\frac{\partial \dot{G}}{\partial T} = -\frac{\partial^2 G}{\partial \boldsymbol{\sigma}\partial T} : \dot{\boldsymbol{\sigma}} - \frac{\partial^2 G}{\partial T^2}\dot{T} - \sum_{n=1}^{24} \frac{\partial^2 G}{\partial \xi^n \partial T}\dot{\xi}^n \tag{25}$$

which, after substituting Eq. (3) into Eq. (25), gives the rate of change of specific entropy as

$$\rho\dot{s} = \boldsymbol{\alpha} : \dot{\boldsymbol{\sigma}} + \frac{\rho c}{T}\dot{T} - \beta\sum_{n=1}^{24}\dot{\xi}^n \tag{26}$$

Substituting Eq. (26) into Eq. (24), the final form of the first law is obtained as

$$\rho c\dot{T} = \sum_{n=1}^{24}\left(-\frac{\partial G}{\partial \xi^n} + \beta T\right)\dot{\xi}^n - T\boldsymbol{\alpha} : \dot{\boldsymbol{\sigma}} - \mathrm{div}\boldsymbol{q} + \rho\hat{g} \tag{27}$$

The energy balance (27) is used for finding the volumetric heat generation in SMAs as

$$\mathscr{R} = \sum_{n=1}^{24}\left(-\frac{\partial G}{\partial \xi^n} + \beta T\right)\dot{\xi}^n - T\boldsymbol{\alpha} : \dot{\boldsymbol{\sigma}} = \sum_{n=1}^{24}(f_n + \beta T)\dot{\xi}^n - T\boldsymbol{\alpha} : \dot{\boldsymbol{\sigma}} \tag{28}$$

where the term f_n is defined in Eq. (4). It is worth noting that during the phase transformation the consistency condition implies that $f_n = f^{\pm}$, where $f^{+} = f^{am}$ for the forward phase transformation and $f^{-} = f^{ma}$ for the reverse transformation. Comparing Eq. (28) with the expression assumed by Lim and McDowell [22], it is observed that Eq. (28) can be simplified to the volumetric heat generation obtained by Lim and McDowell [22] by ignoring the second term that corresponds to the heat generation related to the rate of change of stress and also ignoring the temperature dependency of the coefficient that relates the heat generation to the rate of change of martensitic volume fraction.

The volumetric heat generation $\mathscr{R}$ is given to the finite element model in a user subroutine (UMAT). The numerical solution needs the derivatives of the volumetric heat generation with respect to the temperature and strain. For calculating the derivative of $\mathscr{R}$, we use the variation of the volumetric heat generation, which, after some manipulations, is given as

$$\begin{aligned}\delta\mathscr{R} = {} & \frac{1}{\Delta t}\left[(f^{\pm} + \beta T)\sum_{n=1}^{24}\frac{\partial \Delta\xi^n}{\partial \Delta\boldsymbol{\epsilon}} - \boldsymbol{\alpha} : \frac{\partial \Delta\boldsymbol{\sigma}}{\partial \Delta\boldsymbol{\epsilon}}T\right]\delta\boldsymbol{\epsilon} \\ & + \frac{1}{\Delta t}\left[\beta\sum_{n=1}^{24}\xi^n - \boldsymbol{\alpha} : \Delta\boldsymbol{\sigma} - \boldsymbol{\alpha} : \frac{\partial \Delta\boldsymbol{\sigma}}{\partial \Delta T}T + (f^{\pm} + \beta T)\sum_{n=1}^{24}\frac{\partial \Delta\xi^n}{\partial \Delta T}\right]\delta T\end{aligned} \tag{29}$$

where $\partial\Delta\boldsymbol{\sigma}/\partial\Delta T$ and $\partial\Delta\boldsymbol{\sigma}/\partial\Delta\boldsymbol{\epsilon}$ are the thermal and mechanical Jacobians given in Eq. (15) and Eq. (13), respectively. The terms $\partial\Delta\ \xi^n/\partial\Delta T$ and $\partial\Delta\xi^n/\partial\ \Delta\boldsymbol{\epsilon}$ are given in Eq. $(16)_2$ and Eq. $(14)_2$, respectively. Substituting these parameters into Eq. (29) gives the derivatives of the volumetric heat generation with respect to temperature and strain as

$$\begin{aligned}\partial\Delta\mathscr{R}/\partial\Delta T = {} & \beta\sum_{n=1}^{24}\xi^n - \boldsymbol{\alpha} : \Delta\boldsymbol{\sigma} - \boldsymbol{\alpha} : \mathbb{S}^{-1} : \left(-\sum_{m=1}^{24}\frac{\partial \Delta\boldsymbol{\epsilon}^m}{\partial \Delta T}\right)T \\ & + (f^{\pm} + \beta T)\sum_{m,n=1}^{24}\Gamma_{nm}^{-1}\frac{\partial F^m}{\partial \Delta T},\end{aligned} \tag{30}$$

$$\begin{aligned}\partial\Delta\mathscr{R}/\partial\Delta\boldsymbol{\epsilon} = {} & (f^{\pm} + \beta T)\sum_{m,n=1}^{24}\Gamma_{nm}^{-1}\frac{\partial F^m}{\partial \Delta\boldsymbol{\epsilon}} \\ & - \boldsymbol{\alpha} : \mathbb{S}^{-1} : \left(\mathbb{I} - \sum_{m=1}^{24}\frac{\partial \Delta\boldsymbol{\epsilon}^m}{\partial \Delta\boldsymbol{\epsilon}}\right)T\end{aligned} \tag{31}$$

It is worth noting that in the numerical algorithm the summations with the volume fraction increment in Eqs. (28), (31) and (30) are only written on the q active variants for which the volume fraction is changing during the current increment.

4. Finite element modeling

The constitutive equations, the mechanical and thermal Jacobians, the volumetric heat generation, and the derivatives of volumetric heat generation with respect to temperature and strain are implemented in an appropriate user subroutine (UMAT) in the finite element program ABAQUS. The subroutine is written in a local coordinate system. In the finite element model, a separate local orientation is assigned to the elements in each grain. Details of assigning the crystal orientations for textured

and untextured samples are given in Section 4.2. All the orientation-dependent parameters are transformed to the local coordinates before passing them into the subroutine, and transformed back to the global coordinates when the subroutine results are given to the finite element code. We use the material properties given by Lim and McDowell [22]. These properties are obtained from differential scanning calorimetry tests and the manufacturer's data for a commercial SMA used in the experiments by Lim [21]. The elastic constants (Lamé parameters) are $\lambda = 69.2$ GPa and $\mu = 46.2$ GPa. The critical transformation energies are $f^{am} = 17 \times 10^6$ J m^{-3} and $f^{ma} = 7 \times 10^6$ J m^{-3}. The mass density is $\rho = 6500$ Kg m^{-3} and the chemical energy coefficient is $\beta = 0.6 \times 10^6$ J m^{-3} °C^{-1}. The thermal expansion coefficient is $\alpha_{ij} = \alpha\delta_{ij}$, where $\alpha = 22 \times 10^{-6}$/K [17].[4]

4.1. Grain-scale modeling based on Voronoi tessellations

In the previously reported works in the literature that study polycrystalline SMAs using micromechanical based models, the polycrystal structure was designed for resembling the microstructure to the actual structure as closely as possible (see Fig. 2 in [22] and Fig. 5 in [44]). In these works hexagonal prisms and cubes are used for modeling the geometry of each grain which are far from the actual grains shapes. We use a more realistic microstructure in the finite element model for simulating polycrystal SMAs.

Voronoi tessellations are widely accepted to model polycrystalline aggregates as they provide a realistic approximation of the actual microstructure of non-uniform grain shapes [5,9,46,41]. Voronoi cells are constructed from a set of randomly positioned points (called the generators or Poisson points) in the given domain. Each Voronoi cell is the set of all points in the given set whose distances from the corresponding generator are not greater than their distances from the other generators. Recently, novel frameworks have been introduced for developing finite element (FE) models based on Voronoi tessellations to generate polycrystalline grain structures for micromechanics simulations [40,41]. We use four different Voronoi tessellations for modeling polycrystalline samples subjected to uniaxial loading and bending in this paper. The microstructure and finite element meshes of these models are shown in Fig. 1.

The cubic model shown in Fig. 1a consists of 100 grains. Each side of this cube is $a = 250$ μm, which, after considering the number of grains along each side, results in a mean grain size of 50 μm that is consistent with the optical micrographs of NiTi [10]. We use two models with different numbers of grains, as shown in Fig. 1b and c for studying the uniaxial tension and also bending. The polycrystalline structure in Fig. 1b is $38 \times 75 \times 250$ μm and contains a total of 26 grains. The polycrystalline sample in Fig. 1c is $150 \times 300 \times 1000$ μm and is constructed by 357 grains. Another sample with a circular cross-section is also used for studying the uniaxial tension, as shown in Fig. 1d. This model is constructed by 172 grains with a length and radius of $L = 1000$ and $r = 70$ μm. The selected dimensions in all these models result in a mean grain size of 50 μm. Linear solid tetrahedral elements are used for constructing the FE model (C3D4 and C3D4T). The finite element meshes of the beams are shown in Fig. 1. Periodic boundary conditions are not used in this paper. For nodes lying on the back face perpendicular to the loading direction ($z = 0$), the axial component of displacement is constrained and one node at the corner is fixed in all directions to prevent the rigid body motions. For the bending studies, the nodes in the clamped surface are constrained in all directions.

4.2. FE modeling of textured and untextured samples

In order to study the effect of texture on the bending response of NiTi, we consider two different distributions of crystal orientations in the grains. For modeling the untextured material, a random orientation is assigned to each grain. For modeling the textured material, the results of texture analysis on a drawn bar using an X-ray diffraction are used [11,10]. The experimental pole figures resulting from the X-ray analysis show that the [1 1 1] directions of the crystal lattice among all the grains are predominantly parallel to the axial direction (the z direction in Fig. 1), while the [0 0 1] directions of the crystal lattice are randomly distributed [11,22]. In the finite element model, for modeling the textured material, all the elements in each grain are assigned an orientation such that the [1 1 1] direction of all the orientations is scattered along the axis based on a Gaussian distribution with standard deviation of 10°, while the [0 0 1] directions are randomly distributed. In order to verify the distribution of crystal orientations in the microstructure, we use the orientations in all the grains and calculate the orientation distribution functions for plotting the pole figures corresponding to each sample. These pole figures are compared with the experimental data to make sure that the modeled texture is in agreement with the measured data. As an example, the pole figures obtained from the crystal orientations in all the grains for the sample with 357 grains (Fig. 1c) is shown in Fig. 2. Comparing these figures with the experimental data presented by Gall and Sehitoglu [11] shows that the texture in the material is modeled accurately.

5. Numerical results

Several different case studies are presented in this section for analyzing various aspects of the mechanical and thermomechanical response of polycrystalline NiTi SMAs. In

[4] The compliance and thermal expansion tensors are anisotropic for single crystal monoclinic martensitic NiTi. However, experimentally measured values for the anisotropic material properties of NiTi are not available and these properties can be assumed isotropic with an acceptable accuracy, particularly when the inelastic response is studied [44].

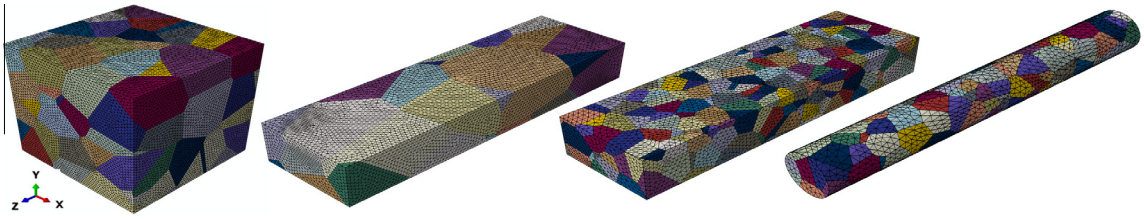

Fig. 1. The finite element mesh of polycrystalline SMAs with (a) 100 grains, (b) 26 grains, (c) 357 grains and (d) 172 grains.

sections 5.1, 5.2, and 5.3 we ignore the thermomechanical coupling by neglecting the effect of phase transformation latent heat. In these sections the loading and unloading processes are assumed to be isothermal. It is shown that ignoring the latent heat and assuming an isothermal process is valid when the material has enough time for exchanging the generated or absorbed heat with the ambient. This is the case for slow loadings or ambient conditions with high convection coefficients at the surfaces [28]. The thermomechanical coupling is studied in Section 5.4. It will be shown that the latent heat generated by the phase transformation causes a rate dependency in the response of polycrystalline SMAs. It is also shown that the latent heat affects the martensite propagation between the grains of a polycrystalline NiTi SMA.

5.1. The role of texture

In this section the role of texture on the mechanical response of polycrystalline SMAs is studied. As mentioned earlier, the role of texture on tension–compression asymmetry has been studied extensively in the literature. The uncoupled constitutive model of this paper was used by Gall and Sehitoglu [11] for studying the stress–strain behavior of textured and untextured polycrystalline NiTi subjected to tension vs. compression. The microstructure of the polycrystal is not modeled in this work and the constitutive equations are solved for a cluster of 2000 grains with different crystallographic orientations by calculating the transformation strain corresponding to each orientation and summing the transformation strains for all the relevant orientations. With this method, only the global stress–strain response is modeled, and the distribution of solution parameters in a polycrystal cannot be studied. However, by using several experiments, Gall and Sehitoglu [11] showed the capability and accuracy of this micromechanical model for studying the role of texture on the tension–compression asymmetry of polycrystalline SMAs. Gall et al. [10] and Lim and McDowell [22] used finite element modeling for studying textured polycrystalline NiTi SMAs. In these works, a simplified geometry was chosen for modeling the microstructure by assuming identical hexagonal prisms as grains in the polycrystal. The role of texture and the rate dependency based on a simplified thermomechanical coupled model were studied. Thamburaja and Anand [44] studied the effect of crystallographic texture on the response of polycrystalline SMAs using a crystal-mechanics-based constitutive model and the finite element simulation. The microstructure in the polycrystal is modeled by assuming all the grains as cubes. In this section we use the polycrystalline models based on the Voronoi tessellations for studying the rule of texture on the mechanical response of NiTi SMAs. As the first step, the effect of texture on the tension–compression asymmetry is studied by considering a polycrystalline sample shown in Fig. 1a. Details of the finite element simulation and modeling the crystal orientations for textured and untextured samples are given in Section 4. The stress–strain responses for textured and untextured NiTi in tension and compression are given in Fig. 3. The stress–strain response for a

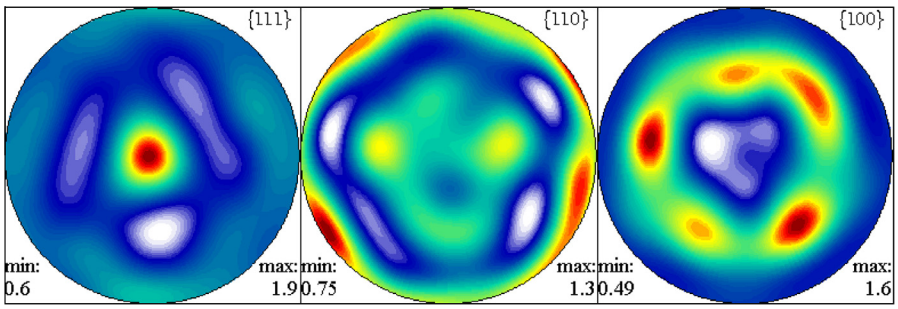

Fig. 2. The {111}, {110} and {100} pole figures obtained from the crystal orientations in the grains of the sample shown in Fig. 1c.

single grain (modeled using one cubic element with periodic boundary conditions) with the [1 1 1] crystal orientation along the loading direction is also shown in Fig. 3b for comparison purposes.

As shown in Fig. 3, while the tension–compression response is almost symmetric for the polycrystalline NiTi with random distribution of grain orientations, the response is significantly asymmetric for the textured polycrystal. It is observed that the phase transformation is slightly more favorable in compression compared to tension for the untextured material as shown in Fig. 3a. This result is in agreement with the previously reported studies of polycrystalline SMAs based on Taylor models [33], self-consistent models [11], and micromechanical models in conjunction with simplified finite element simulations [10]. The stress–strain curves for a textured polycrystal and a [1 1 1]-oriented single crystal are shown in Fig. 3b. As observed earlier, the crystallographic texture is the origin of tension–compression asymmetry in polycrystalline SMAs, and this phenomenon is reflected in the similarity between the single crystal and textured polycrystalline responses [12], as shown in Fig. 3b. The tension–compression asymmetry for the [1 1 1]-oriented single crystal can be explained theoretically by considering the Schmid factors of the most favorably oriented martensite variant for uniaxial compression and tension directions, which are 0.27 and 0.39, respectively [36,13]. It is worth noting that, in modeling the textured polycrystalline SMAs in Gall et al. [10], the [1 1 1] crystallographic direction of the grains are randomly wobbled around the loading direction within tolerances of 0–5 or 0–10 degrees. However, as explained in Section 4.2, in the present work we use a Gaussian distribution for modeling the textured polycrystal. This is more realistic and has the capability of modeling different textures more accurately by changing the standard deviation in the distribution. By using a Gaussian distribution with a relatively small standard deviation (10° in the present work) for the crystallographic directions, the stress–strain curves of the polycrystal are more similar to the response of a single [1 1 1]-oriented crystal compared to a random distribution between 0° and 10°. This happens because in the Gaussian distribution with small standard deviations most of the orientations are aligned near the [1 1 1] direction, while for a random distribution they are freely distributed between 0° and 10°. Comparing the results of the present work with those of Gall et al. [10], we observe that the difference between the response of a single crystal and a polycrystal is more significant in Gall et al. [10]. However, the present model is capable of modeling various textures accurately by choosing appropriate standard deviations in the Gaussian distribution.

Comparing the simulation results in Fig. 3b with the experimentally measured stress–strain curves for polycrystal and single crystal NiTi reported by Gall et al. [12], it is clear that the present model is predicting the key features of the response accurately. Consistent with the experiments, the model predicts a slight decrease in the critical transformation stress for the polycrystal compared to the single crystal. Decreasing the stress levels for a polycrystal is more prominent in compression, which is consistent with the experimental observations. This can also be explained based on transformation Schmid factor arguments [36,10]. It is worth noting that a similar study was presented by Gall et al. [10], and the stress–strain curves for a single crystal and a polycrystal were compared. As mentioned earlier, the structure of grains in the polycrystal is modeled assuming a uniform shape for all the grains. The simulation results in Gall et al. [10] show that the stress–strain curves are not sensitive to the number of grains; the results are not affected by increasing the number of grains. This finding was also used by Lim and McDowell [22] for concluding that a single mesh and microstructure is adequate for studying the general response of polycrystalline SMAs. However, we will show in the present work that the rapid convergence of results by increasing the number of grains in the previous works is due to the

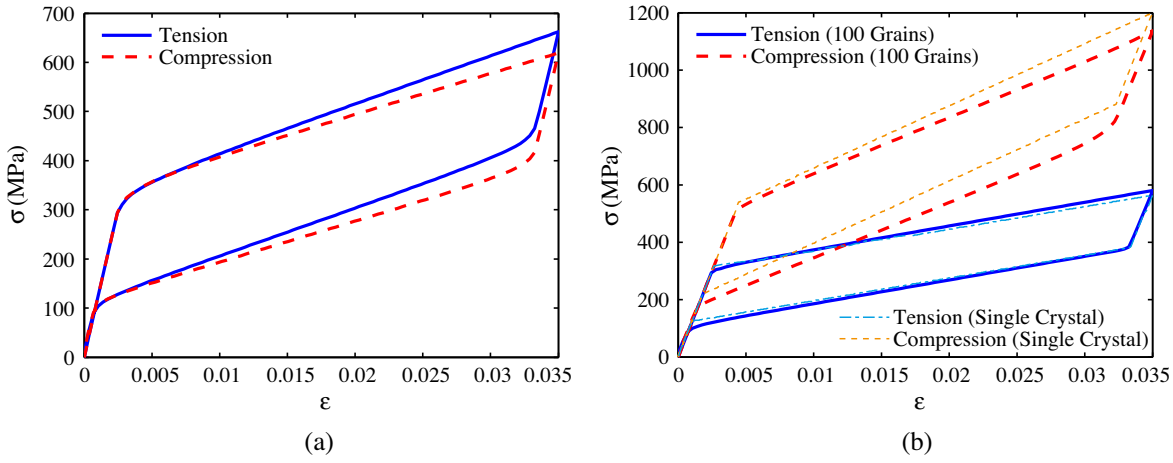

Fig. 3. Comparison of the stress–strain response in tension and compression for (a) untextured and (b) textured NiTi polycrystal model with 100 grains as shown in Fig. 1a.

assumption of uniformity of the grain shapes. We will show in the next section that, for the accurate microstructure representation used in this paper, the material response is highly affected by the number of grains, which can be understood as a size effect.

5.2. The size effect

In this section, the effect of size (or the number of grains) on the response of textured and untextured polycrystalline SMAs is studied. The stress–strain curves for a cubic polycrystal shown in Fig. 1a are presented in Section 5.1. In this section we study the uniaxial tension and compression for the polycrystal models shown in Fig. 1b and c. As mentioned in Section 4.1, the model of Fig. 1b contains a total of 26 grains and by considering a mean grain size of 50 μm the size of this model is 38 × 75 × 250 μm. The polycrystal model in Fig. 1c is 150 × 300 × 1000 μ m and contains 357 grains. The results in this section can also be compared with the curves in the previous section for a cubic model with 100 grains. However, one should notice that the number of grains along the loading axis and in the cross-section for the models of this section are different from the cubic model in the previous section and the results cannot be compared directly. We will also study the response of a single crystal with [1 1 1] direction along the loading axis for comparison purposes.

The stress–strain curves for the uniaxial loading of polycrystalline SMAs in tension and compression are shown in Fig. 4. The uniaxial stress–strain curves for untextured models are shown in Fig. 4a. It is observed that the difference between tensile and compressive responses is more prominent for the larger model with 357 grains. Comparing the results in this figure with those of Fig. 3a shows that the difference between tensile and compressive responses is remarkably larger for the rectangular cuboid models of Fig. 1b and c compared to the cubic model of Fig. 1a. This shows that not only the number of grains in the micromechanical model but also the shape of the sample can affect the mechanical response of polycrystalline SMAs.

The stress–strain curves for the textured polycrystalline samples are shown in Fig. 4b. Similar to the cubic model with 100 grains, for both sizes considered in this section the difference between the tensile and compressive responses is remarkably larger for the NiTi polycrystal with a dominant ⟨1 1 1⟩ fiber texture compared to the polycrystal with a random distribution of orientations. Fig. 4b for the textured polycrystal NiTi shows that, while the tensile response is not highly affected by the size, the compressive response is remarkably different for the small and large textured polycrystal samples. This phenomenon can be explained by considering the stress–strain curves for a single [1 1 1]-oriented crystal (shown with thin lines in the figure). As discussed in the previous section, the Schmid factor arguments explain the effect of adding more grains with [1 1 1] orientations around the loading direction on increasing the difference in tensile and compressive responses. As seen in Fig. 4a and b, in the model with 26 grains, the textured polycrystal contains a small number of grains with [1 1 1] orientation and the response is moved slightly from an untextured sample toward the single [1 1 1]-oriented crystal. However, adding a large number of grains with [1 1 1] orientation along the loading axis in the model with 357 grains leads to a stress–strain curve similar to that of the single crystal. The important observation is that the compressive response is more sensitive to the size (or the number of grains) compared to the tensile response. It is worth noting that we are not considering the thermomechanical coupling in this section and the size effect studied here does not originate from the size dependence of exchanging the latent heat with the ambient that was previously studied in the macroscale [28]. Also, it should be noted that periodic boundary conditions are not imposed and our simulations correspond to the mechanical response of NiTi micropillars with free surfaces. Conducting experiments on some NiTi micropillars for studying the size

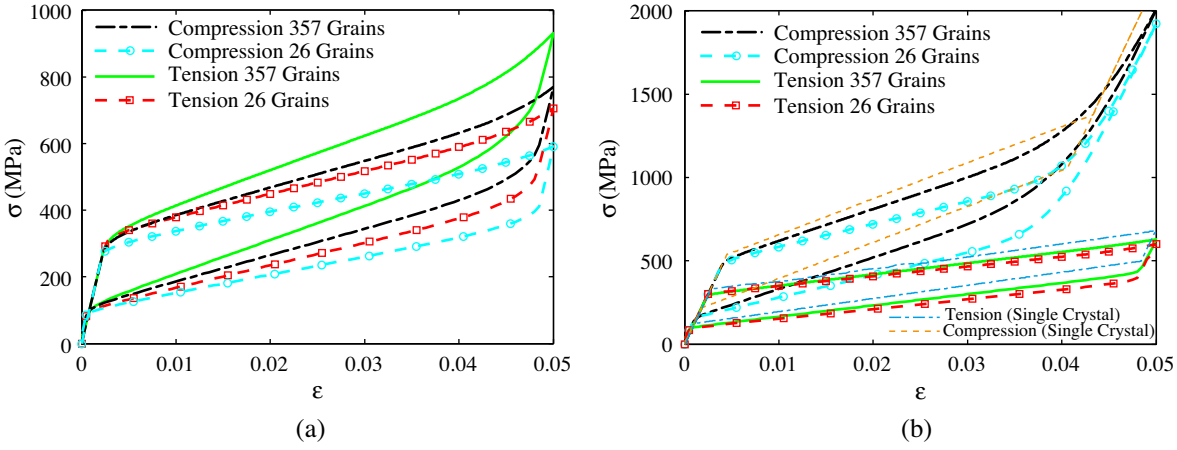

Fig. 4. The effect of size on the stress–strain response in tension and compression for (a) untextured and (b) textured NiTi polycrystal models with 26 and 357 grains, as shown in Fig. 1.

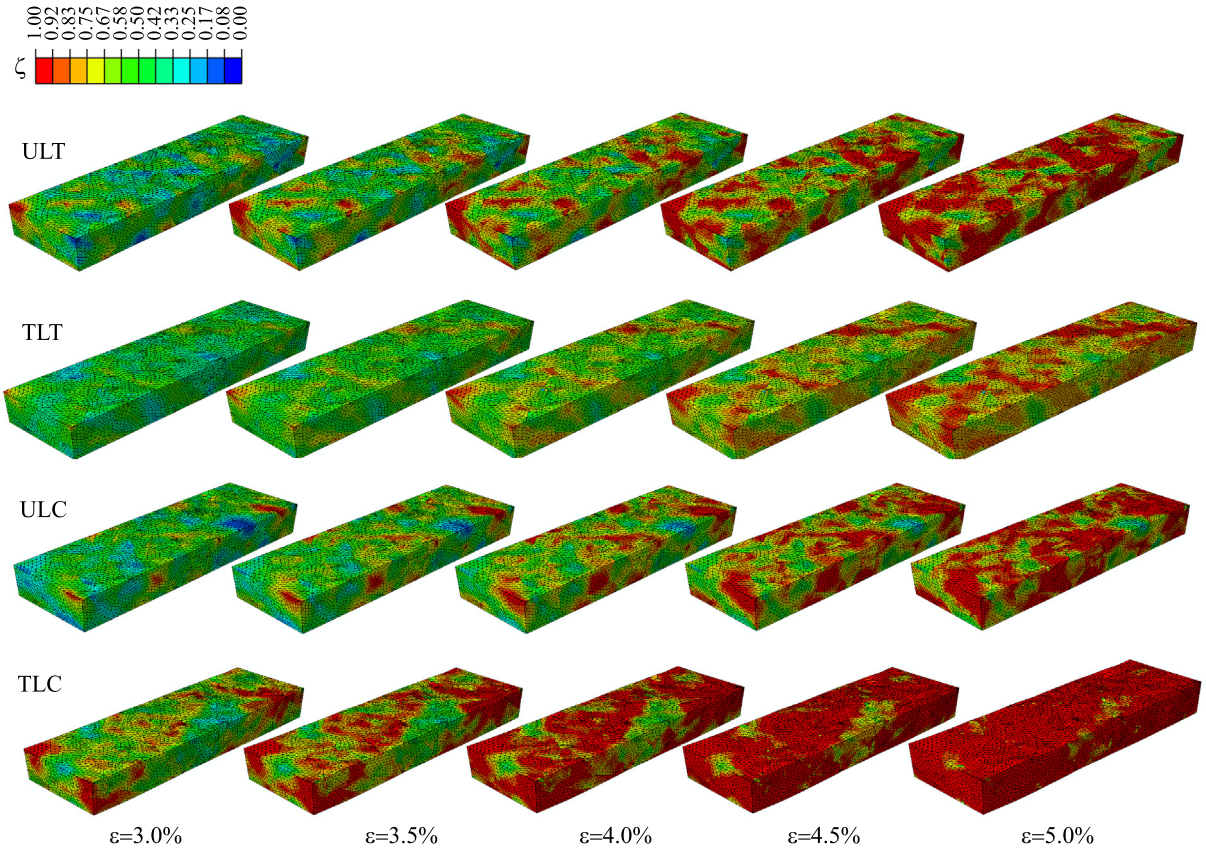

Fig. 5. The initiation and propagation of martensite in textured and untextured NiTi polycrystalline model with 357 grains subjected to 5% tensile and compressive strain. The three-letter labels stand for texture (U for untextured and T for textured), size (L for large and S for small model) and loading (T for tension and C for compression), respectively.

effect and validating the theoretical observations will be the subject of a future communication.

To further understand the effect of size and texture on the response of polycrystalline SMAs, the distribution of martensitic volume fraction is also studied. The initiation and propagation of martensite during forward phase transformation (austenite to martensite) are studied for small and large models with 26 and 357 grains in tension and compression. In each case, both random and textured distributions of crystallographic orientations are studied. In order to label the contour plots in this section, we use a three-letter code, in which the first letter stands for the texture (U for untextured and T for textured crystallographic orientations), the second letter defines the size (L for the larger model with 357 grains and S for smaller model with 26 grains) and the third letter represents the loading (T for tension and C for compression). For comparison purposes, a uniform color coding is selected in all the contour plots in Figs. 5 and 6, in which red represents martensite and blue shows austenite. The propagation of martensitic volume fractions in large polycrystalline NiTi samples for strains between 3 and 5% are shown in Fig. 5. The same results for the smaller model with 26 grains are shown in Fig. 6.

Comparing the contour plots in Figs. 5 and 6 shows that the martensitic volume fraction is strongly affected by the texture, the number of grains and the stress state. Comparing the first two rows in Fig. 5 shows that, while the phase transformation initiates from a large number of grains distributed in the sample for the large polycrystal subjected to tension with random orientation of grains (ULT), in the large textured sample subjected to tension (TLT) the phase transformation initiates in a limited number of grains with more favorable crystallographic directions for phase transformation in tension. Comparing tensile and compressive responses of these models in Fig. 5 reveals an important effect of texture on the martensite propagation in polycrystalline SMAs. Comparing the tensile and compressive responses for the untextured large samples (ULT and ULC) shows that the phase transformation propagates similarly for both stress states. However, the same comparison for the textured samples (TLT and TLC) shows that the spatial spread of phase transformation is remarkably more rapid under compression. It is worth noting that the spatial spread of phase transformation initiation in textured polycrystal samples is more rapid in tension compared to compression, as shown by Gall et al. [10]. They studied the phase transformation initiation (at least 0.05% martensite was assumed as the initiation of phase transformation), and it was observed that the number of grains in which the phase transformation has been started is larger in tension than in compression at equal strains. This is consistent with the stress–strain response shown in

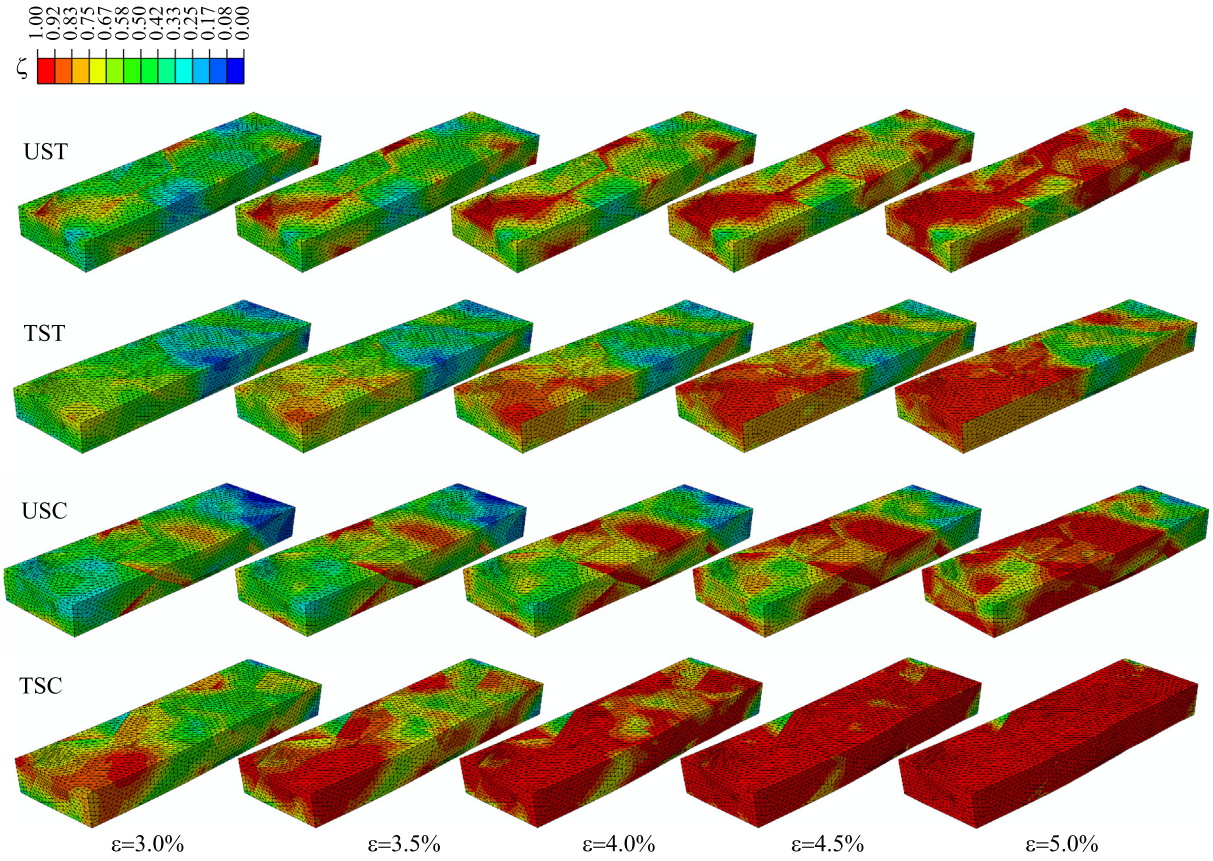

Fig. 6. The initiation and propagation of martensite in textured and untextured NiTi polycrystalline model with 26 grains subjected to 5% tensile and compressive strain. The three-letter labels stand for texture (U for untextured and T for textured), size (L for large and S for small model) and loading (T for tension and C for compression), respectively.

Fig. 4 because the phase transformation initiation occurs at lower strain values for tensile loading. However, we are studying the contour plots of the martensitic volume fraction and, as shown in this section, the spatial spread of grains with a full transformation from austenite to martensite (shown with red in the contour plots) is more rapid in compression. This result is also consistent with the stress–strain curves shown in Fig. 4 where the phase transformation is completed for smaller strains in compression compared to tension. As shown in Fig. 4a, the compressive and tensile responses for the untextured material are similar. This is the reason for observing a similar propagation of martensitic volume fractions in ULT and ULC models (Fig. 5). The martensitic volume fraction distributions for smaller samples (with 26 grains) are shown in Fig. 6. The grain boundaries are distinguished more clearly in this figure (see Fig. 1b for a better view of the grain boundaries).

Comparing the untextured and textured small samples in tension (UST and TST in Fig. 6) shows that the phase transformation initiates from more grains in the untextured material. Also, it is observed that in the untextured samples (both UST and USC in Fig. 6) the phase transformation initiation from the grain boundaries is more prominent compared to the textured polycrystal samples. This happens because in the untextured samples there are several boundaries between grains with a large mismatch between the crystallographic orientations, while in the textured samples the orientations in adjacent grains are more likely similar. It can be concluded that the initiation of phase transformation from the grain boundaries plays a more important rule in the untextured material compared to the textured case. Comparing the tensile and compressive responses for the textured and untextured samples shows that the spatial distributions of phase transformation are similar for the large and small samples.

Comparing the results in Figs. 5 and 6 shows that the number of grains (or size) has a strong effect on the phase transformation propagation in polycrystalline SMAs. As shown in these figures, the role of phase transformation initiation at the grain boundaries is more prominent in the small samples and the spread of the fully transformed regions is affected by the number of grains. This difference in the phase transformation propagation is related to the size effect observed in the stress–strain responses (Fig. 4).

5.3. Bending analysis of microscaled beams

In this section the numerical results for bending analysis of textured and untextured polycrystalline SMA beams are presented. The FE models are shown in Fig. 1b and c. All the nodes in one end are constrained in all directions and a transverse displacement is applied to the nodes in the other

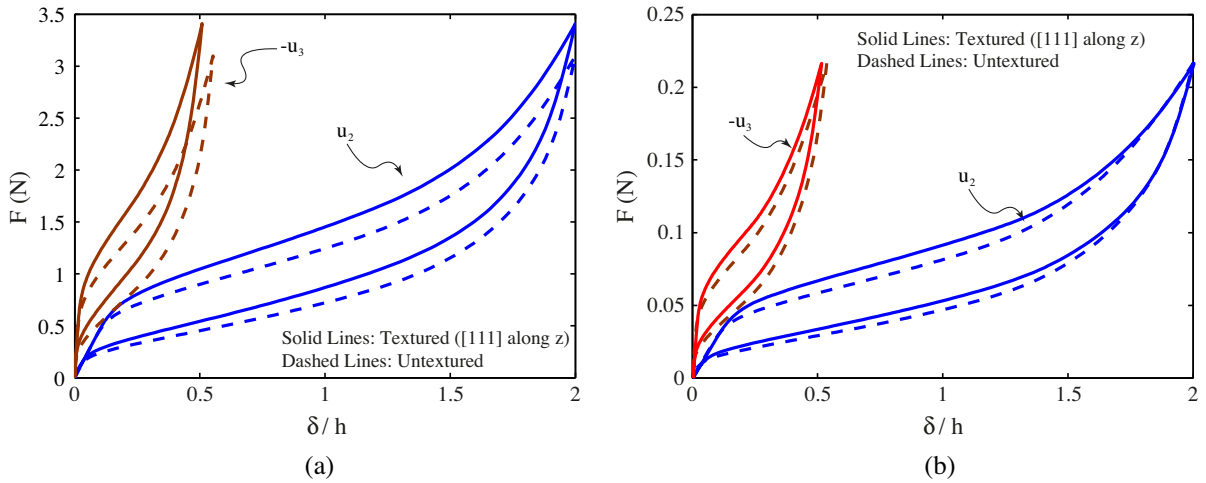

Fig. 7. In-plane and transverse tip deflection for a polycrystalline beam subjected to bending. The response of textured and untextured beams are compared for polycrystal structures with (a) 26 grains and (b) 357 grains.

end. The final transverse deflection δ is set such that $\delta/h = 2$ for both beams, where h is the thickness. The loading phase is then followed by an unloading phase that is modeled by setting the deflection to zero. The geometrical nonlinearity is considered in the FE solution for studying both the transverse and in-plane deflections. The reaction forces at the clamped nodes are computed and summed for obtaining the total reaction force during loading–unloading. The force–deflection response of the beams with 26 and 357 grains are shown in Fig. 7a and b, respectively. In both cases of coarse and fine grains, the texture effect is studied by comparing the response of a beam with texture vs. an untextured beam with random crystal orientations.

Comparing parts (a) and (b) of Fig. 7 shows that the effect of texture on the force–deflection response is more significant in the polycrystalline beam with a large number of grains. The force–deflection response for the smaller beam with 26 grains is almost identical for the textured and untextured crystal orientations. We consider the polycrystal structure with 357 grains for studying the stress and martensitic volume fraction distribution in the beams subjected to bending in the following. All the distributions correspond to the loading phase with $\delta/h = 1.5$. The martensitic volume fraction (summation of volume fraction of all active martensite variants) is shown in Fig. 8. The volume fraction distributions in textured and untextured beams are shown in Fig. 8a and b, respectively. Comparing the volume fraction distribution near the clamped edge in these figures shows the asymmetric distribution of matrensite volume fraction in the textured beam. It was previously shown that, while an untextured NiTi polycrystalline response is semi-symmetric in tension–compression, the tensile and compressive responses are remarkably different in a textured polycrystal [11]. As mentioned in Section 5.1, this happens because in the textured material the majority of grains are oriented along the [1 1 1] crystallographic direction, which is soft under tensile loading and hard under compression. In the untextured samples the crystallographic directions are randomly distributed, which leads to an almost symmetric response in tension–compression. As shown in Fig. 8a, the neutral axis position (marked with a red arrow on the figure) is shifted towards the

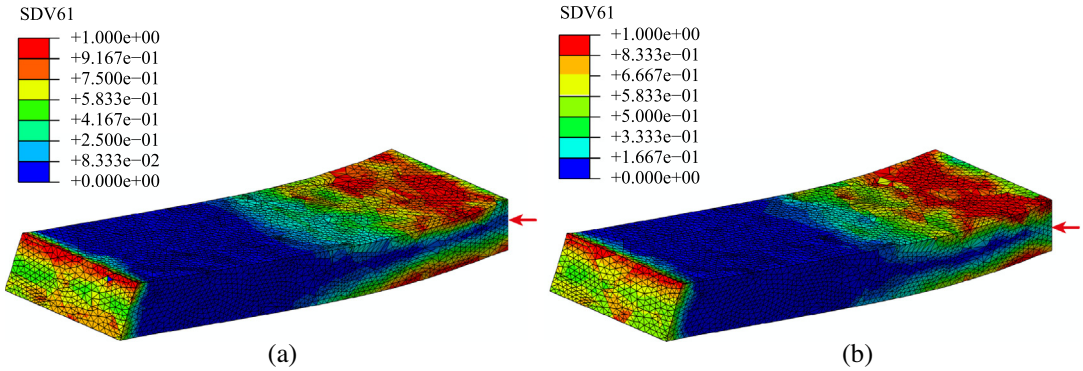

Fig. 8. Martensitic volume fraction distribution in a polycrystalline beam with 357 grains subjected to bending with (a) textured and (b) untextured crystal orientations.

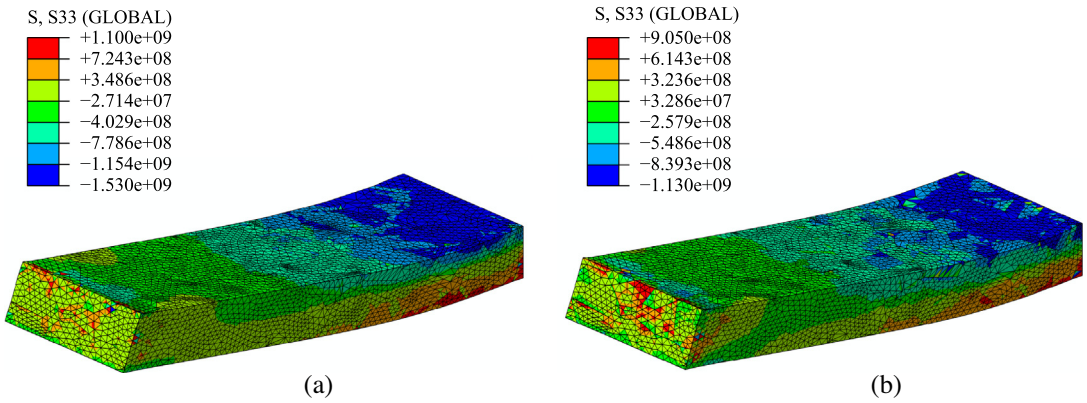

Fig. 9. Normal stress distribution in a polycrystalline beam with 357 grains subjected to bending with (a) textured and (b) untextured crystal orientations.

compressive part of the cross-section for the textured beam, while it is near the center line for the untextured beam due to the symmetry in tension–compression response. The response of macro-SMA beams subjected to bending was studied previously by the authors based on phenomenological constitutive frameworks [31]. Comparing the results of this section with those presented in Mirzaeifar et al. [31] shows that the J_2-based phenomenological models are suitable for modeling the response of untextured polycrystalline materials, whereas $J_2 - I_1$-based models can be used for studying the textured polycrystal SMAs in bending with an acceptable accuracy.

The normal stress distribution is compared for the textured and untextured beams in Fig. 9a and b. An asymmetry in the stress distribution for the textured material is observed. It can also be observed that the maximum compressive stress is remarkably larger than the maximum tensile stress in the textured beam, which is consistent with the stress–strain curves obtained in Section 5.1.

5.4. Thermomechanical coupling in polycrystalline SMAs

In this section the effect of phase transformation latent heat is considered and the thermomechanical response of textured and untextured polycrystalline SMAs is studied. In the previous numerical case studies, an isothermal loading–unloading process was assumed, which is valid when the phase transformation latent heat can be exchanged with the ambient and the material temperature is constant during the whole process. In this section we consider the latent heat effect and also the temperature changes due to generation or absorption of latent heat in forward or reverse phase transformation as explained in Section 3. As mentioned earlier, our model considers a more accurate description for the rate of latent heat generation and its derivatives with respect to strain and temperature compared to the simplified works previously reported in the literature [7,22]. Also, the more accurate micromechanical model based on Voronoi tessellations sheds some light on the effect of thermomechanical coupling on the propagation of phase transformation in polycrystalline NiTi.

In this section, a polycrystalline model with circular cross-section is used. This model with 172 grains is shown in Fig. 1d. The details of the finite element model and mechanical boundary conditions are similar to those of the previous case studies in Section 4. Continuous solid tetrahedral elements with added temperature degrees of freedom (C3D4T) are used. The initial temperature is

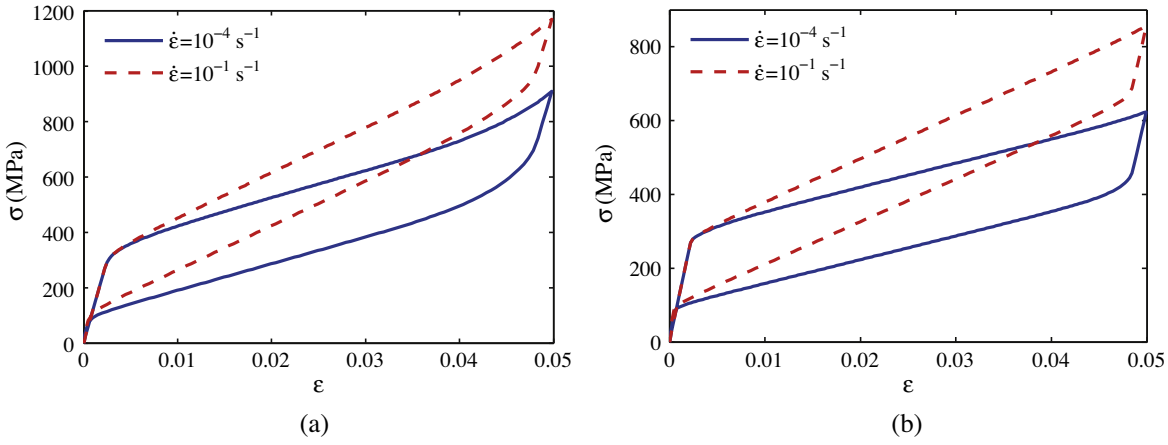

Fig. 10. The effect of loading rate by considering the thermomechanical coupling on the stress–strain response of (a) untextured and (b) textured polycrystalline NiTi samples (the micromechanical model is shown in Fig. 1d).

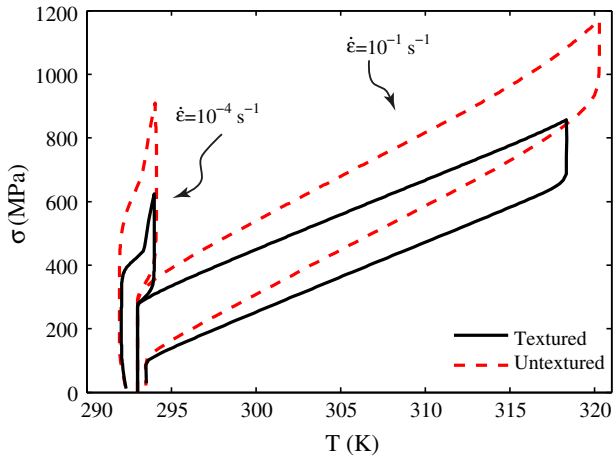

Fig. 11. Average temperature of untextured and textured polycrystalline NiTi samples subjected to slow and fast loadings.

$T_0 = 293$ K and the material is austenite initially. Free convection with heat transfer coefficient $h_\infty = 10$ W/m^2 K is considered at the sides of the sample. Two different loading rates of $\dot{\epsilon} = 10^{-4}$ and 10^{-1} s^{-1} are studied for simulating the near isothermal and near adiabatic cases, respectively. The polycrystal average stress–strain curves for these two loading rates are shown in Fig. 10 for untextured and textured samples.

As shown in Fig. 10, in the vicinity of thermomechanical coupling, the loading rate has a significant effect on the mechanical response of both samples with textured and random distributions of crystal orientations. Comparing the stress–strain curves for slow and fast loadings in each case shows that the maximum stresses at the end of the loading phase are increased by 29.8% and 37.8% in fast loading for untextured and textured samples, respectively. For the fast loading, $\dot{\epsilon} = 10^{-1}$ s^{-1}, the slope of stress–strain curve is increased and the hysteresis area is slightly decreased for both untextured and textured samples. These observations are both consistent with similar responses at the macroscale NiTi samples studied by a phenomenological constitutive framework by ignoring the micromechanical structure [28], and also experimental results for large polycrystalline SMA samples [3]. The average temperature of the polycrystal during loading–unloading is studied in Fig. 11. The temperature at all the integration points is averaged for calculating the parameter T in this figure.

As expected, the temperature change in slow loading is negligible while a significant temperature change is observed in fast loading $\dot{\epsilon} = 10^{-1}$ s^{-1}. Fig. 11 shows that, during loading for the strain rate $\dot{\epsilon} = 10^{-1}$ s^{-1}, the temperature increase in the textured material is larger at a specific stress (the temperature increases from 297 to 309 K at $\sigma = 800$ MPa in the untextured sample, while it increases to 316 K at the same stress level in the textured sample). However, the temperature change in the untextured sample is larger at the same strain compared to the textured material (at the end of loading with $\epsilon = 0.05$ the temperature is increased to 318 K in the textured material, while the temperature in the untextured sample is 320 K). The temperature changes are consistent with the results obtained from phenomenological constitutive equations for polycrystalline SMAs at large scales [28]. As shown in Fig. 11, the average temperature of the sample is lower than the initial temperature at the end of loading for the slow loading rate. This phenomenon is also observed in the calculations based on the phenomenological constitutive equations. This effect can be explained as follows [28]. As shown in Fig. 10, at the beginning of unloading, before the start of reverse phase transformation, phase transformation does not occur. During this step, the phase transformation heat is not generated and the material is cooling due to convective heat exchange with the ambient. This temperature loss is followed by heat absorption during reverse phase transformation and causes the material to be colder than the initial and ambient temperatures at the end of the unloading phase.

The effect of thermomechanical coupling and the latent heat on the propagation of phase transformation in the polycrystalline material is studied next. We consider the textured sample subjected to slow and fast loadings. The stress–strain curves for this sample are shown in Fig. 10b. The martensitic volume fraction distributions at the end

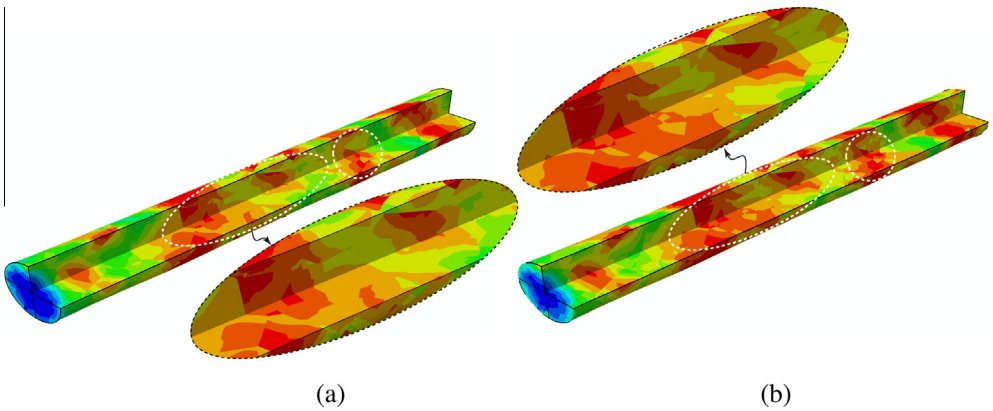

Fig. 12. The martensitic volume fraction distributions at the end of the loading phase in the textured polycrystalline SMA samples subjected to (a) fast and (b) slow loadings (the stress–strain curves are shown in Fig. 10b).

of the loading phase in the textured polycrystalline SMA samples are shown in Fig. 12.

Distribution of the martensitic volume fraction in the sample subjected to fast loading is shown in Fig. 12a. Two cuts along the length of the sample are used to show the distribution inside the sample (the micromechanical model is shown in Fig. 1d). Fig. 12b shows the same results for the slow loading rate. Two sample regions with the highest martensitic volume fraction values are marked by dashed white lines in both figures. For comparison purposes, a larger view of one of these regions is also shown for both fast and slow loading rates. It is clear that the loading rate affects the distribution of phase transformation. In both marked regions in the figure, the phase transformation is distributed in a larger area in the sample subjected to slow loading.

6. Conclusions

A constitutive model based on the micromechanics of single crystals of SMAs is used for studying the pseudoelastic response of polycrystalline SMAs subjected to uniaxial and bending loads. By introducing a set of martensitic volume fractions corresponding to each active variant, the total transformation strain is obtained as a function of stress-free transformation strains of 24 CVPs obtained from the crystallographic data for NiTi. Compared to the available micromechanical-based models in the literature, an improved coupled thermomechanical framework is introduced for polycrystalline SMAs by coupling the energy balance equation obtained from the first law of thermodynamics to the mechanical constitutive equations. The microstructure of polycrystalline SMAs is simulated accurately by using Voronoi tessellations in a three-dimensional finite element model and various samples with different number of grains and shapes are modeled for studying various aspects of the thermomechanical response of polycrystalline NiTi SMAs. The effect of crystallographic texture on the thermomechanical response of NiTi is studied by assigning appropriate crystallographic orientations in the grains. The interaction between the stress state (tensile or compressive), size (modeled by considering samples with different number of grains) and crystallographic texture on the mechanical response and phase transformation propagation in polycrystalline SMAs is analyzed. The bending response of polycrystalline micropillars is also studied, and the effect of size and crystallographic texture on the bending response is analyzed. Using the coupled thermomechanical framework for polycrystalline SMAs, the effect of loading rate and the phase transformation latent heat on the response of textured and untextured NiTi samples is studied. It is shown that the temperature changes due to the heat generation during phase transformation can affect the propagation of martensite in samples subjected to high strain rates.

Acknowledgments

The authors are grateful to Dr. Igor Simonovski for providing the geometrical models with Voronoi tessellations.

References

[1] Anand L, Gurtin ME. Thermal effects in the superelasticity of crystalline shape-memory materials. J Mech Phys Solids 2003;51(6):1015–58.
[2] Anand L, Kothari M. A computational procedure for rate-independent crystal plasticity. J Mech Phys Solids 1996;44(4):525–58.
[3] Auricchio F, Fugazza D, Desroches R. Rate-dependent thermomechanical modelling of superelastic shape-memory alloys for seismic applications. J Intell Mater Syst Struct 2008;19(1):47–61.
[4] Auricchio F, Taylor RL, Lubliner J. Shape-memory alloys: macromodelling and numerical simulations of the superelastic behavior. Comput Methods Appl Mech Eng 1997;146:281–312.
[5] Boots B. The arrangement of cells in random networks. Metallography 1982;15(1):53–62.
[6] Buchheit TE, Wert JA. Modeling the effects of stress state and crystal orientation on the stress-induced transformation of NiTi single crystals. Metall Mater Trans A – Phys Metall Mater Sci 1994;25:2383–9.
[7] Entemeyer D, Patoor E, Eberhardt A, Berveiller M. Strain rate sensitivity in superelasticity. Int J Plasticity 2000;16(10):1269–88.
[8] Frick CP, Ortega AM, Tyber J, Gall K, Maier HJ. Multiscale structure and properties of cast and deformation processed polycrystalline NiTi shape-memory alloys. Metall Mater Trans A: Phys Metall Mater Sci 2004;35A(7):2013–25.
[9] Fritzen F, Böhlke T, Schnack E. Periodic three-dimensional mesh generation for crystalline aggregates based on Voronoi tessellations. Comput Mech 2009;43:701–13.
[10] Gall K, Lim TJ, McDowell DL, Sehitoglu H, Chumlyakov YI. The role of intergranular constraint on the stress-induced martensitic transformation in textured polycrystalline NiTi. Int J Plasticity 2000;16(10–11):1189–214.
[11] Gall K, Sehitoglu H. The role of texture in tension–compression asymmetry in polycrystalline NiTi. Int J Plasticity 1999;15(1):69–92.
[12] Gall K, Sehitoglu H, Anderson R, Karaman I, Chumlyakov YI, Kireeva IV. On the mechanical behavior of single crystal NiTi shape memory alloys and related polycrystalline phenomenon. Mater Sci Eng A 2001;317(1–2):85–92.
[13] Gall K, Sehitoglu H, Chumlyakov Y, Kireeva I. Tension–compression asymmetry of the stress–strain response in aged single crystal and polycrystalline NiTi. Acta Mater 1999;47(4):1203–17.
[14] Hane K, Shield T. Microstructure in the cubic to monoclinic transition in titaniumnickel shape memory alloys. Acta Mater 1999;47(9):2603–17.
[15] Idesman A, Levitas V, Preston D, Cho J-Y. Finite element simulations of martensitic phase transitions and microstructures based on a strain softening model. J Mech Phys Solids 2005;53(3):495–523.
[16] Kastner O, Ackland GJ. Mesoscale kinetics produces martensitic microstructure. J Mech Phys Solids 2009;57(1):109–21.
[17] Lagoudas DC. Shape memory alloys: modeling and engineering applications. New York: Springer; 2008.
[18] Leclercq S, Lexcellent C. A general macroscopic description of the thermomechanical behavior of shape memory alloys. J Mech Phys Solids 1996;44(6):953–80.
[19] Levitas VI, Idesman AV, Preston DL. Microscale simulation of martensitic microstructure evolution. Phys Rev Lett 2004;93:105701.
[20] Liang C, Rogers CA. The multi-dimensional constitutive relations of shape memory alloys. J Eng Math 1992;26:429–43.
[21] Lim T. Behavior of a NiTi shape memory alloy under cyclic proportional and nonproportional loading. Ph.D. Thesis. Georgia Institute of Technology, Atlanta, Georgia; 1999.

[22] Lim T, McDowell D. Cyclic thermomechanical behavior of a polycrystalline pseudoelastic shape memory alloy. J Mech Phys Solids 2002;50(3):651–76.
[23] Liu J-Y, Lu H, Chen J-M, Zhang Z. Finite element simulation of martensitic transition based on thermo-mechanical model. Mater Sci Eng: A 2007;448(1–2):204–9.
[24] Lu Z, Weng G. A self-consistent model for the stress–strain behavior of shape-memory alloy polycrystals. Acta Mater 1998;46(15):5423–33.
[25] Marketz F, Fischer F. A micromechanical study on the coupling effect between microplastic deformation and martensitic transformation. Comput Mater Sci 1994;3(2):307–25.
[26] Marketz F, Fischer F. Modelling the mechanical behavior of shape memory alloys under variant coalescence. Comput Mater Sci 1996;5(1–3):210–26.
[27] Matsumoto O, Miyazaki S, Otsuka K, Tamura H. Crystallography of martensitic transformation in Ti–Ni single crystals. Acta Metall 1987;35(8):2137–44.
[28] Mirzaeifar R, Desroches R, Yavari A. Analysis of the rate-dependent coupled thermo-mechanical response of shape memory alloy bars and wires in tension. Contin Mech Thermodynam 2011;23(4):363–85.
[29] Mirzaeifar R, Desroches R, Yavari A. A combined analytical, numerical, and experimental study of shape-memory-alloy helical springs. Int J Solids Struct 2011;48(3–4):611–24.
[30] Mirzaeifar R, Desroches R, Yavari A, Gall K. Coupled thermo-mechanical analysis of shape memory alloy circular bars in pure torsion. Int J Non-Linear Mech 2012;47(3):118–28.
[31] Mirzaeifar R, Desroches R, Yavari A, Gall K. On superelastic bending of shape memory alloy beams. Int J Solids Struct 2013;50(10):1664–80.
[32] Nishida M, Itai I, Kitamura K, Chiba A, Yamauchi K. Effect of grain size of parent phase on twinning modes of b19' martensite in an equiatomic Ti–Ni shape memory alloy. J Phys IV: JP 1995;5(8 pt):C8–635.
[33] Ono N, Satoh A, Ohta H. Discussion on the mechanical properties of shape memory alloys based on a polycrystal model. Mater Trans JIM 1989;30(10):756–64.
[34] Panico M, Brinson L. A three-dimensional phenomenological model for martensite reorientation in shape memory alloys. J Mech Phys Solids 2007;55(11):2491–511.
[35] Patoor E, Eberhardt A, Berveiller M. Micromechanical modelling of superelasticity in shape memory alloys. J Phys IV 1996;6(1). C1-277–C1-292.
[36] Patoor E, Elamrani M, Eberhardt A, Berveiller M. Determination of the origin for the dissymmetry observed between tensile and compression tests on shape-memory alloys. J Phys IV 1995;5(C2):495–500.
[37] Peultier B, Zineb TB, Patoor E. Macroscopic constitutive law for SMA: application to structure analysis by FEM. Mater Sci Eng: A 2006:454–8.
[38] Qidwai MA, Lagoudas DC. On thermomechanics and transformation surfaces of polycrystalline NiTi shape memory alloy material. Int J Plasticity 2000;16(10):1309–43.
[39] Sehitoglu H, Karaman I, Anderson R, Zhang X, Gall K, Maier H, et al. Compressive response of NiTi single crystals. Acta Mater 2000;48(13):3311–26.
[40] Simonovski I, Cizelj L. The influence of grains crystallographic orientations on advancing short crack. Int J Fatigue 2007;29(9–):2005–14.
[41] Simonovski I, Cizelj L. Automatic parallel generation of finite element meshes for complex spatial structures. Comput Mater Sci 2011;50(5):1606–18.
[42] Sun QP, Hwang KC. Micromechanics modelling for the constitutive behavior of polycrystalline shape memory alloys II. Study of the individual phenomena. J Mech Phys Solids 1993;41(1):19–33.
[43] Tanaka K, Nishimura F, Hayashi T, Tobushi H, Lexcellent C. Phenomenological analysis on subloops and cyclic behavior in shape memory alloys under mechanical and/or thermal loads. Mech Mater 1995;19:281–92.
[44] Thamburaja P, Anand L. Polycrystalline shape-memory materials: effect of crystallographic texture. J Mech Phys Solids 2001;49(4):709–37.
[45] Thamburaja P, Anand L. Superelastic behavior in tensiontorsion of an initially-textured Ti–Ni shape-memory alloy. Int J Plasticity 2002;18(11):1607–17.
[46] Zhang P, Balint D, Lin J. An integrated scheme for crystal plasticity analysis: virtual grain structure generation. Comput Mater Sci 2011;50(10):2854–64.
[47] Zhang X, Sehitoglu H. Crystallography of the B2 → R → B19' phase transformations in NiTi. Mater Sci Eng: A 2004;374(1–2):292–302.